Journal of Materials Chemistry C

PAPER

View Article Online
View Journal | View Issue

Cite this: J. Mater. Chem. C, 2015, 3, 5233

Photoluminescence of $CsMI_3:Eu^{2+}$ (M = Mg, Ca, and Sr) – a spectroscopic probe on structural distortions

Markus Suta and Claudia Wickleder*

Received 23rd February 2015,
Accepted 14th April 2015

DOI: 10.1039/c5tc00515a

www.rsc.org/MaterialsC

The photoluminescence of Eu^{2+} ions doped in iodidoperovskites, $CsMI_3$ (M = Mg, Ca, Sr), was studied. Eu^{2+} occupies the alkaline earth site in each of these compounds. The emission spectra of the doped perovskites are characterized by $4f^65d^1 \rightarrow 4f^7$ transitions of Eu^{2+} located in the yellow range for $CsMgI_3$ and the blue range for $CsCaI_3$ and $CsSrI_3$, respectively. All excitation spectra provide a well-resolved fine structure arising from different ^7F_J (J = 0,...,6) levels of the $4f^6$ core of the excited state configuration, indicating a weak exchange interaction with the 5d electron. The decay times and temperature dependence of the luminescence were also analyzed. Both $CsMgI_3:Eu^{2+}$ and $CsSrI_3:Eu^{2+}$ show a redshifted emission with respect to $CsCaI_3:Eu^{2+}$. This is explained by trigonal distortions of the $[EuI_6]^{4-}$ octahedra in the former two compounds. The energetic order of the resulting crystal field states is justified in terms of the angular overlap model of ligand field theory. This series of Eu^{2+} doped earth alkaline iodidoperovskites may serve as a textbook example for the detailed understanding of the structure–luminescence relationships of Eu^{2+} ions, which is very important for tailoring functional materials for respective applications.

1. Introduction

The luminescence of Eu^{2+} has been a topic in many papers and reviews due to its broad-banded 4f–5d transitions that are parity allowed and thus interesting for many applications like, *e.g.* LEDs or detectors such as scintillators and X-ray storage phosphors. The nature of the 5d orbitals and their interaction with the local crystal field afford a systematic impact upon the emission color of the respective Eu^{2+}-activated material. For example, in fluorides, such as CaF_2 and SrF_2, Eu^{2+} shows violet emission,[1] whereas in $KMgF_3$, the 5d states are located at higher energies such that 4f–4f line emission from the excited ^6P_J and ^6I_J states is also observed in the UV range.[2,3] On the other hand, in nitridosilicates such as $M_3Si_6O_{12}N_2:Eu^{2+}$ (M = Sr, Ba),[4] $M_2Si_5N_8:Eu^{2+}$ (M = Ca, Sr, Ba)[5] or $MSi_2O_2N_2:Eu^{2+}$ (M = Ca, Sr),[6,7] Eu^{2+} shows yellow to orange luminescence. Further examples include Eu^{2+}-activated CaS or SrS, showing a red emission.[8] The examples mentioned above show how the luminescence of Eu^{2+} can be affected only by varying the composition of the host material. Interesting reviews that summarize and discuss the data of many of the Eu^{2+}-activated compounds presented in the literature were published by Rubio[9] and Dorenbos[10] during the last two decades.

Both for basic research and applications in high-energy radiation detection, halides are interesting host materials for Eu^{2+}. As already described above, many of the studies presented in the literature have been attempted for fluorides, and chlorides have already been subject to many investigations. Unlike Eu^{2+}-activated fluorides, however, the heavier halides only exhibit broad-banded 5d–4f emission in the violet to blue range due to the nephelauxetic effect shifting the position of the barycenter of the $4f^65d^1$ states below the lowest excited $4f^7$ state. Moreover, crystal field splitting shifts the lowest $4f^65d^1$ state yet to lower energies, as was indicated by Blasse.[11] Typical examples from the literature are $MZnCl_4:Eu^{2+}$ (M = Sr, Ba), which emit at 402 nm and 396 nm, respectively.[12] Similar to the results presented in this paper, Gahane *et al.* presented the optical properties of Eu^{2+} ions doped in the ternary chlorides $CsMCl_3$ (M = Mg, Ca, Sr).[13] Many other chlorides are presented in ref. 10 and references given therein.

The number of reported Eu^{2+}-activated bromides, however, is already very small and mainly includes detailed investigations of the binary alkali and alkaline earth halides.[10] More recently, however, several ternary bromides and iodides have attracted a lot of attention due to their potential application as scintillating materials. Typical examples for bromides as scintillators include $CsCaBr_3:Eu^{2+}$ [14] and $CsSrBr_3:Eu^{2+}$.[15,16] A detailed analysis of the photoluminescence properties of Eu^{2+} in the series $CsMBr_3$ (M = Mg, Ca, Sr) has been recently published by us.[17] Their range of applicability of these materials is, however, limited due to their high sensitivity against moisture.

Inorganic Chemistry, Faculty of Science and Engineering, University of Siegen, 57068 Siegen, Germany. E-mail: wickleder@chemie.uni-siegen.de; Fax: +49-271-740-2555; Tel: +49-271-740-4217

In contrast to the rest of the halides, the luminescence of Eu^{2+} doped in ternary iodides is currently only described in a superficial manner in the literature.[10] Recently, the applicability of $CsMI_3$ (M = Ca, Sr) as scintillators has been investigated and presented by the group of Melcher.[18–21] Due to the higher covalence of Eu–I bonds compared to other halides, the 5d–4f emission is described to shift to lower energies and thus located in the blue or even bluish-green region.[10] Since the iodides described in this paper mainly contain heavy ions, their applicability as scintillating materials seems absolutely plausible, as the previously mentioned publications also nicely illustrate. The higher doping concentrations of Eu^{2+} required for applications result in a loss of resolution of the spectra and thus do not allow a detailed analysis of the fine structure. These features are, however, important for a basic understanding of the structure–luminescence relationship. Another aim of this paper is to demonstrate the photoluminescence of Eu^{2+} doped in $CsMgI_3$, which has not been presented so far in the literature.

To the best of our knowledge, no detailed analysis of the Eu^{2+}-activated ternary iodides $CsMI_3$ (M = Mg, Ca, Sr) with emphasis on the systematics of the photoluminescence properties in correlation with the structures and chemical compositions of these compounds has been attempted before. Moreover, it seems interesting to us to compare the properties of Eu^{2+} in iodides with those of the bromides of similar composition. Such an analysis is very important also from an application perspective as it allows the predictability and tunability of the photoluminescence properties of Eu^{2+} by distinct changes in the size of the site the Eu^{2+} ions occupy as well as in the structural features of a compound. This is not only interesting for scintillating materials but also very important for other applications such as in LED technology.

2. Experimental

2.1. Preparation

CsI (Merck, 99.5%) was dried at 200 °C in a dynamic vacuum in order to remove any traces of moisture. The anhydrous iodides MI_2 (M = Ca, Sr) could be obtained by first dissolving the respective hydrates $CaI_2{\cdot}4H_2O$ (Acros Organics, 99%) and $SrI_2{\cdot}xH_2O$ (Heraeus, 99.5%) in concentrated HI (Acros Organics, 57 wt%) to remove traces of MCO_3 (M = Ca, Sr) that may form upon standing of the hydrates in air. The thus obtained pure hydrates of the iodides were then dried in a dynamic vacuum at 200 °C to obtain pure anhydrous iodides. EuI_2 was prepared from Eu_2O_3 (smart elements, 99.995%) using the ammonium iodide route in order to avoid any traces of moisture and oxygen.[22] After slow decomposition at a heating rate of 4 °C h^{-1} of the thus prepared ternary compound $(NH_4)_3EuI_6{\cdot}xH_2O$ to 300 °C in a dynamic vacuum, EuI_2 was directly obtained as a slightly yellowish powder. The phase purity of all starting materials was checked by X-ray powder diffraction (Siemens D5000, Cu K_α radiation).

The doped ternary iodides $CsMI_3$:Eu^{2+} (M = Ca, Sr) were prepared by fusing the respective starting materials CsI and MI_2 (M = Ca, Sr) at their corresponding molar ratios together with 0.1 mol% EuI_2 in sealed silica ampoules under vacuum using the Bridgman technique. For $CsMgI_3$:Eu^{2+}, CsI_3 (Alfa Aesar, 98%), Mg metals (smart elements, 99.8%) and 0.1 mol% EuI_2 were used as starting materials instead. All mixtures were heated at a rate of 20 °C h^{-1} to their respective melting points and kept in the melt for 36 h. The mixtures were then slowly recrystallized (2 °C h^{-1}) to 100 °C below their melting points

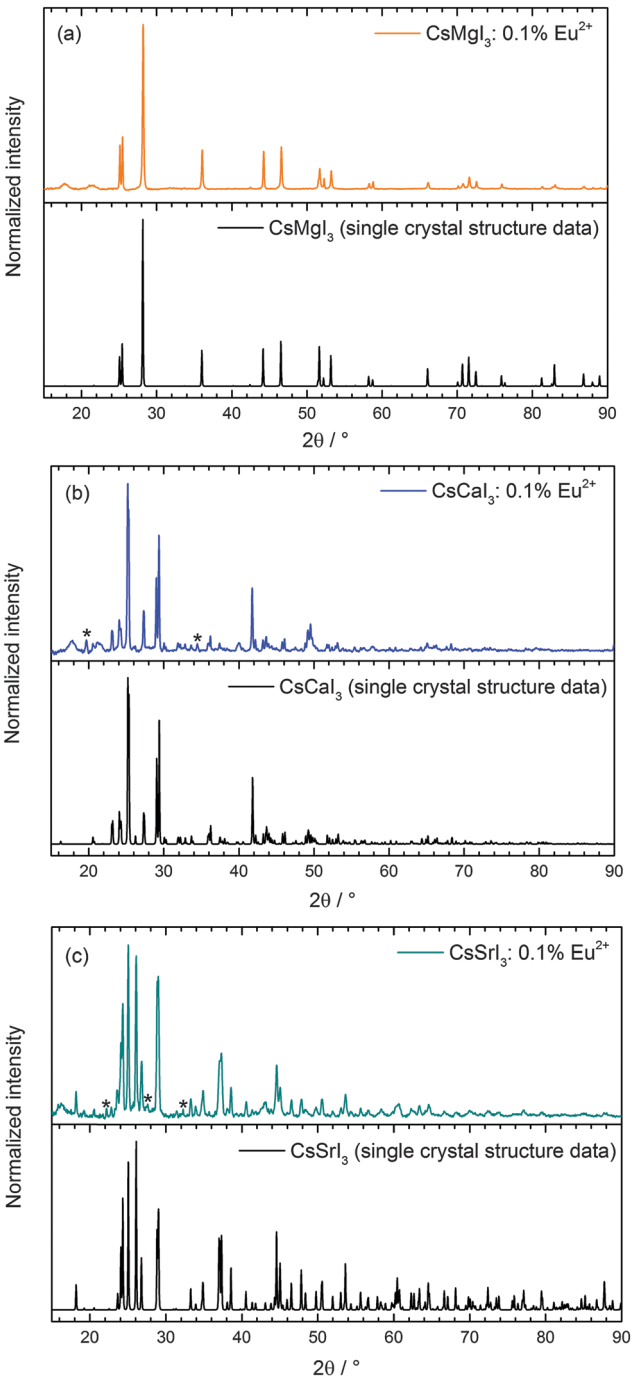

Fig. 1 Measured X-ray powder diffraction patterns of (a) $CsMgI_3$:0.1% Eu^{2+}, (b) $CsCaI_3$:0.1% Eu^{2+} and (c) $CsSrI_3$:0.1% Eu^{2+} in comparison to the respective patterns according to the literature.[23,24] The marked references denote the *in situ* formation of hydrates during the XRD measurements.

and finally cooled to room temperature at 10 °C h^{-1}. The phase purity and crystallinity of the products were also verified by X-ray powder diffraction (see Fig. 1). Due to the hygroscopic nature and sensitivity to oxygen of all the previously described compounds, every step had to be performed under a dry Ar atmosphere using a glove box (Braun).

2.2. Optical measurements

Photoluminescence emission and excitation spectra were obtained using a Fluorolog3 spectrofluorometer (Jobin Yvon) equipped with a 450 W xenon lamp and double Czerny–Turner monochromators allowing a resolution down to 0.05 nm and a photomultiplier detection system R928P (Hamamatsu) coupled with a photon counting system. A liquid helium closed-cycle cryostat was used to perform temperature-dependent measurements at 10 K. The emission spectra were corrected for photomultiplier sensitivity and the excitation spectra were corrected for lamp intensity. For decay time measurements, a frequency-tripled Nd:YAG laser (Spectra Physics Quanta Ray Indi 40) with a repetition rate of 10 Hz and a pulse width of 8 ns was used (λ_{ex} = 355 nm). For the detection of the desired emission wavelength, a single monochromator (Jobin Yvon) was employed that allows a resolution down to 5 nm. The decay signal was recorded using a photomultiplier tube that was attached to an oscilloscope (Tektronix, 500 kHz).

3. Results

3.1. Crystal structures and coordination spheres of $CsMI_3$ host lattices (M = Mg, Ca, Sr)

The crystal structures of all iodides presented in this paper can be derived from the perovskite structure and have already been described in the literature.[23,24] The measured powder diffraction patterns are depicted in Fig. 1 and indicate the phase purity of the synthesized compounds. Due to the fact that the XRD measurements could not be performed without the total exclusion of air, some other reflections reveal an increase in intensity after every subsequent measurement on the same samples. These reflections can be assigned to the *in situ* formation of hydrates of the respective iodides due to their hygroscopic nature in air. Moreover, all XRD patterns reveal the presence of broad reflections in the range between 2θ = 15° and 22°, which is an artifact due to the fixation of the powders with silicon grease. No effects of doping with EuI_2 can be detected as it is expected due to the very low concentration of only 0.1 mol% that is below the sensitivity limit of the XRD device. Hence, no change in the crystal structures of the three iodides is induced by doping of EuI_2.

The symmetry data and average M–I distances (M = Mg, Ca, Sr) important for the discussion of the luminescence spectra are summarized in Table 1.

$CsMgI_3$ crystallizes in the $CsNiCl_3$ structure type, which is a hexagonally distorted variation of the perovskite type structure with the space group $P6_3/mmc$ (no. 194).[23] The average Mg–I distance is 2.90 Å and the structure is depicted in Fig. 2. The Cs^+ ions are 12-fold coordinated by I^- ions in the form of anticuboctahedra whereas the Mg^{2+} ions are six-fold coordinated in the form of octahedra. The local site symmetry of D_{3d} (see Table 1), however, already indicates a severe trigonal distortion. This is induced by the face-sharing pattern of the $[MgI_6]^{4-}$ octahedra that form linear chains along the *c* axis and lead to a high anisotropy of the crystal structure. The effect of anisotropy on the photoluminescence properties of Eu^{2+} has already been discussed in the isostructural compound $CsCdBr_3$.[25,26]

Table 1 Overview of the local site symmetries of the M^{2+} sites and average M–I distances in $CsMI_3$ (M = Mg, Ca, and Sr)[23,24]

Compound	Local site symmetry of M^{2+} site	Average M–I distance/Å
$CsMgI_3$	D_{3d}	2.90
$CsCaI_3$	C_i	3.10
$CsSrI_3$	C_{2h}	3.37

$CsCaI_3$ crystallizes in the orthorhombic $GdFeO_3$ structure type with the space group *Pnma* (no. 62) and is isostructural to $CsSrBr_3$ [24] (see Fig. 3). The average Ca–I distance is 3.10 Å. The Cs^+ ions are (8+2)-fold coordinated by I^- ions and the Ca^{2+} ions are six-fold coordinated by I^- ions in the form of tilted octahedra along the *c* axis with local C_i symmetry (see Table 1). However, the deviation from octahedral symmetry can be assumed to be small, which is a reasonable basis for our interpretation of the luminescence spectra (see Section 4.2).

$CsSrI_3$ crystallizes in a filled $PuBr_3$ structure type, which is characterized by an orthorhombic crystal structure with the

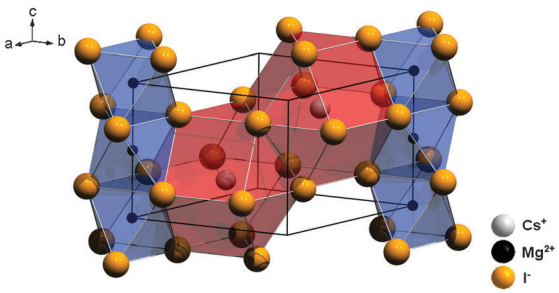

Fig. 2 Representation of the crystal structure of $CsMgI_3$ indicating the anisotropy due to the face-sharing $[MgI_6]^{4-}$ octahedra along the hexagonal *c* axis.[23]

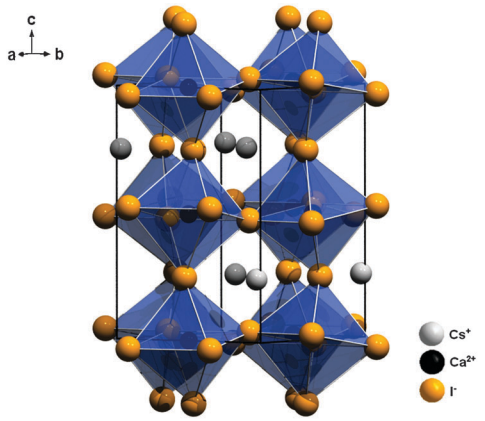

Fig. 3 Representation of the crystal structure of $CsCaI_3$ with emphasis on the slightly tilted $[CaI_6]^{4-}$ octahedra.[24]

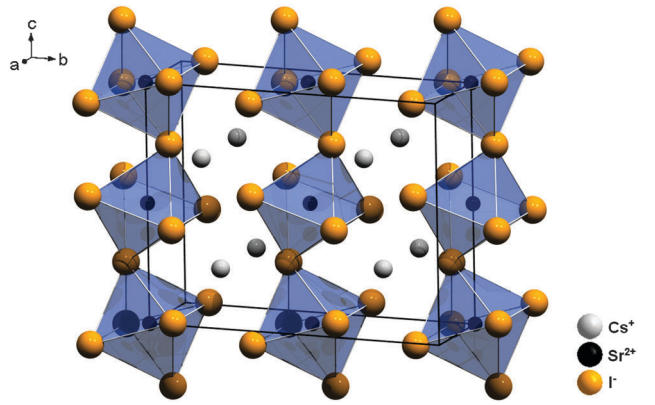

Fig. 4 Representation of the crystal structure of $CsSrI_3$ with indication of the large disposal of the $[SrI_6]^{4-}$ octahedra.[24]

space group *Cmcm* (no. 63)[24] and is depicted in Fig. 4. In this structure, the Cs^+ ions are only 8-fold coordinated by I^- ions in the form of two-fold capped trigonal prisms. The Sr^{2+} ions are six-fold coordinated in the form of tilted octahedra along the *c* axis with local C_{2h} symmetry (see Table 1). The average Sr–I distance is 3.37 Å in this compound.

With regard to different structures, a remarkable development can be noted as the distortion of the $[MI_6]^{4-}$ octahedra (M = Mg, Ca, Sr) increases in the series $CsCaI_3$ < $CsSrI_3$ < $CsMgI_3$ and ends in a face-sharing pattern of the octahedra in $CsMgI_3$. Along with this development, the deviation from a perfect octahedral environment for Eu^{2+} in these three compounds also increases and trigonal distortion has to be taken more into account. We will review this aspect in Section 4.

3.2. Photoluminescence of $CsMI_3$:0.1%Eu^{2+} (M = Mg, Ca, and Sr)

The Eu^{2+}-activated iodides presented in this paper show a bright luminescence upon UV excitation at room temperature, which is the blue region for $CsCaI_3$:Eu^{2+} and $CsSrI_3$:Eu^{2+} and greenish-yellow in the case of $CsMgI_3$:Eu^{2+}. For all three materials, the transitions can be interpreted with the fact that the Eu^{2+} ions occupy exclusively the respective alkaline earth sites. For the respective Eu^{2+}-activated bromides $CsMBr_3$ (M = Mg, Ca, and Sr),[17] we have introduced several energetic values based on the notation and definitions of Dorenbos that afford a more detailed picture of the electronic states of Eu^{2+} in the respective compounds.[10,27,28] We will also use this notation in this paper.

3.3. $CsMgI_3$

$CsMgI_3$:0.1% Eu^{2+} shows a bright yellow luminescence upon UV excitation at room temperature. Low temperature luminescence spectra as well as a photograph of the luminescent sample at room temperature are shown in Fig. 5. To the best of our knowledge, no luminescence properties of Eu^{2+}-activated $CsMgI_3$ have been reported so far. The emission spectrum at 10 K is characterized by a broad asymmetric Gaussian band with a maximum localized at 17 330 cm^{-1} (577 nm). The full width at half maximum of Γ_{10K} = 2430 cm^{-1} is relatively large, indicating a strong electron–phonon coupling. The emission

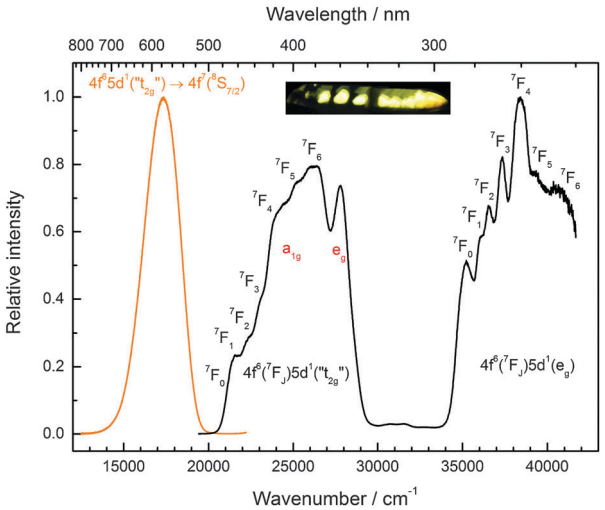

Fig. 5 Emission (orange line, E_{ex} = 24 390 cm^{-1}) and excitation spectrum (black line, E_{em} = 18 020 cm^{-1}) of $CsMgI_3$:0.1% Eu^{2+} at 10 K. Note the splitting of the anticipated "t_{2g}" state into the trigonal field states a_{1g} and e_g. Inset: $CsMgI_3$:0.1% Eu^{2+} showing yellow luminescence upon UV irradiation at room temperature.

band can be assigned to $4f^6 5d^1(t_{2g}) \rightarrow 4f^7(^8S_{7/2})$ transitions of Eu^{2+} substituting for Mg^{2+} ions assuming O_h site symmetry for a first approximation. To a certain extent, the asymmetry of the band can be understood from the large difference in the ionic radii between Eu^{2+} and Mg^{2+} ($r(Eu^{2+})$ = 1.17 Å and $r(Mg^{2+})$ = 0.72 Å).[29] Although the occupation of the Cs^+ site may also be plausible ($r(Cs^+)$ = 1.88 Å),[29] it can be excluded due to the fact that the coordination number is much higher. This would lead to a highly blue-shifted emission and is well established in the scintillator CsI:Eu^{2+}, where the coordination number of the Cs^+ sites is 8 and the respective Eu^{2+} emission is already located at 22 470 cm^{-1} (445 nm).[30] Moreover, we performed EXAFS measurements on the Eu^{2+}-doped isostructural compounds $CsMgCl_3$ and $CsMgBr_3$, which we will publish in another paper. The measurements definitely prove the sole occupation of the Mg^{2+} sites at concentrations below 3%.

The assumption of octahedral site symmetry for the Eu^{2+} ions serves well for a crude interpretation of the luminescence spectra. However, as we will show below, for a more detailed interpretation of the electronic properties of Eu^{2+} in this compound, this approximation is indeed too simplified.

The excitation spectrum of $CsMgI_3$:0.1% Eu^{2+} at 10 K, as shown in Fig. 5, is characterized by two broad bands that contain a detailed fine structure. Their presence is easily understood from the splitting of the 5d orbitals in an octahedral crystal field that gives rise to a "t_{2g}" and an e_g state, the latter being located at higher energy. We marked the t_{2g} state with quotation marks since the assumption of O_h symmetry for Eu^{2+} is too simplified in this case, as we will explain below. The fine structure arises due to the remaining $4f^6$ core in the excited state configuration of Eu^{2+} and can be identified with the different ^7F_J states (J = 0,...,6). Interestingly, the fine structure is also observable in the e_g excitation band. This observation has so far been only reported for the binary alkali halides[31] and Eu^{2+}-activated $CsMBr_3$,[17] but not in the case of other host lattices. It indicates a weak exchange

interaction between the 4f electrons and the 5d electron in the excited state[32] and becomes much less resolved at room temperature. The positions of the different ^7F_J states are compiled in Table 2 and their position relative to the $^7F_0$ state fits well with the values anticipated from Eu^{3+}.[33] The good resolution of the different ^7F_J states allows a relatively precise determination of the Stokes shift $\Delta S(2+,CsMgI_3) = 3870\ cm^{-1}$.

A detailed observation on the excitation spectrum of the Eu^{2+}-related emission depicted in Fig. 5 reveals the presence of another band located at 27 770 cm^{-1} (360 nm). This remarkable feature has already been observed in Eu^{2+}-activated isostructural compounds such as $CsCdBr_3$ [25,26] and $CsMgBr_3$.[17] As we have already indicated in Section 3.1, this can be understood if trigonal distortion of O_h to D_{3d} symmetry (see Table 1) is taken into account leading to a splitting of the anticipated "t_{2g}" state into an a_{1g} and an e_g state. Due to that reason, we will mark the anticipated octahedral field state "t_{2g}" with quotation marks throughout this paper. More conclusions from this effect, *e.g.* the given energetic order of the a_{1g} and the e_g state, will be discussed in Section 4.2. The energetic difference between the a_{1g} and the e_g state is the trigonal crystal field splitting, $\varepsilon_{trig}(7,2+,CsMgI_3) = 4310\ cm^{-1}$.

3.4. $CsCaI_3$

$CsCaI_3$:0.1% Eu^{2+} is characterized by strong blue luminescence upon UV irradiation at room temperature. Fig. 6 depicts the low temperature luminescence spectra as well as a photograph of the luminescent sample at room temperature. It has been recently reported that Eu^{2+}-activated $CsCaI_3$ is a promising scintillator with a light output comparable to NaI:Tl^+.[18,19] The emission shows a slightly asymmetric Gaussian band peaking at 22 370 cm^{-1} (447 nm), which is in very good agreement with the value reported in the literature (450 nm).[18] The full width at half maximum amounts to $\Gamma_{10K} = 640\ cm^{-1}$. The emission can be clearly identified by the $4f^6(^7F_J)5d^1(t_{2g}) \rightarrow 4f^7(^8S_{7/2})$ transition of Eu^{2+} substituting for Ca^{2+} ions under the assumption of an approximate octahedral site symmetry. The difference in ionic radii ($r(Eu^{2+})$ = 1.17 Å and $r(Ca^{2+})$ = 1.00 Å)[29] explains the observed asymmetry of the Gaussian band.

A distinct fine structure is observed in the excitation spectra arising due to the different ^7F_J states from the $4f^6$ core. As there are only two broad bands observed in the excitation spectrum,

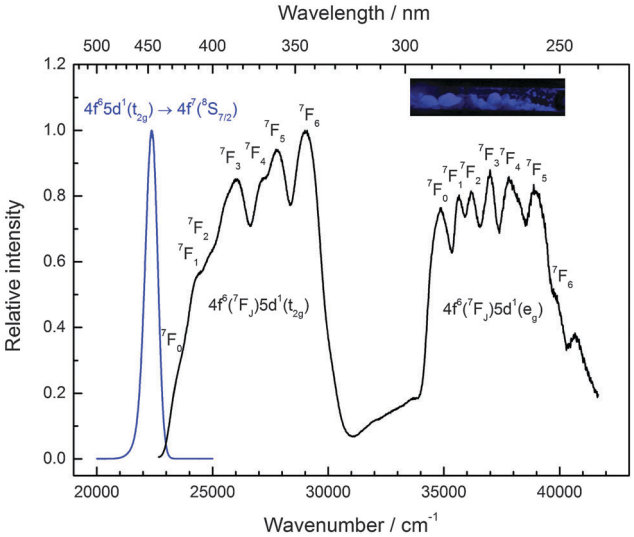

Fig. 6 Emission (blue line, E_{ex} = 25 640 cm^{-1}) and excitation spectrum (black line, E_{em} = 22 470 cm^{-1}) of $CsCaI_3$:0.1% Eu^{2+} at 10 K. Inset: $CsCaI_3$:0.1% Eu^{2+} showing blue luminescence upon UV irradiation at room temperature.

the assumption of an octahedral environment for Eu^{2+} seems legitimate, giving rise to a t_{2g} and an e_g state. Similar to $CsMgI_3$:Eu^{2+} (see Fig. 5), the fine structure is also observable in the e_g state. This indicates, again, a weak exchange interaction between the $4f^6$ electrons and the 5d electron.[32] The positions of the different ^7F_J levels are compiled in Table 3. Within the experimental error, they are in good agreement with the values expected from the respective energies known from Eu^{3+}.[33]

Due to the well-resolved fine structure, it is also possible to determine the Stokes shift accurately, which is $\Delta S(2+,CsCaI_3)$ = 1310 cm^{-1}. The octahedral crystal field splitting, 10 Dq, can be also determined and is given by $\varepsilon_{cfs}(7,2+,CsCaI_3) = 11\,050\ cm^{-1}$ using the nomenclature used by Dorenbos.[10]

3.5. $CsSrI_3$

Similar to Eu^{2+}-activated $CsCaI_3$, $CsSrI_3$:0.1% Eu^{2+} shows blue luminescence upon excitation with UV light at room temperature. The luminescence spectra at 10 K and a photograph of the luminescent sample are shown in Fig. 7. Similar to $CsCaI_3$, Eu^{2+}-activated $CsSrI_3$ also shows efficient radioluminescence and is thus a promising candidate for scintillation materials.[20,21]

Table 2 Positions of the $4f^6(^7F_J)5d^1$ states in $CsMgI_3$:0.1% Eu^{2+} and energy differences ΔE_{J-0} of the $4f^6(^7F_J)5d^1$ (J = 1–6) states relative to the $4f^6(^7F_0)5d^1$ state

$4f^6(^7F_J)5d^1(t_{2g})$			$4f^6(^7F_J)5d^1(e_g)$		
State ^7F_J	Position/ cm^{-1}	$\Delta E_{J-0}/cm^{-1}$	State ^7F_J	Position/ cm^{-1}	$\Delta E_{J-0}/cm^{-1}$
$^7F_0$	21 200	0	$^7F_0$	35 240	0
$^7F_1$	21 700	500	$^7F_1$	36 050	810
$^7F_2$	22 500	1300	$^7F_2$	36 540	1300
$^7F_3$	23 170	1970	$^7F_3$	37 310	2070
$^7F_4$	24 160	2960	$^7F_4$	38 430	3190
$^7F_5$	25 240	4040	$^7F_5$	39 290	4050
$^7F_6$	26 280	5080	$^7F_6$	40 600	5360

Table 3 Positions of the $4f^6(^7F_J)5d^1$ states in $CsCaI_3$:0.1% Eu^{2+} and energy differences ΔE_{J-0} of the $4f^6(^7F_J)5d^1$ (J = 1–6) states relative to the $4f^6(^7F_0)5d^1$ state

$4f^6(^7F_J)5d^1(t_{2g})$			$4f^6(^7F_J)5d^1(e_g)$		
State ^7F_J	Position/ cm^{-1}	$\Delta E_{J-0}/cm^{-1}$	State ^7F_J	Position/ cm^{-1}	$\Delta E_{J-0}/cm^{-1}$
$^7F_0$	23 680	0	$^7F_0$	34 970	0
$^7F_1$	24 350	670	$^7F_1$	35 600	630
$^7F_2$	24 940	1260	$^7F_2$	36 230	1260
$^7F_3$	26 050	2370	$^7F_3$	36 990	2020
$^7F_4$	27 230	3550	$^7F_4$	37 860	2890
$^7F_5$	27 790	4110	$^7F_5$	38 980	4010
$^7F_6$	29 050	5370	$^7F_6$	39 810	4840

The emission band arising from the $4f^6(^7F_J)5d^1 \rightarrow 4f^7(^8S_{7/2})$ transition is an almost perfect Gaussian band with a maximum at 22 010 cm^{-1} (454 nm). The value is in very good agreement with the value found in the literature (452 nm).[20] The full width at half maximum is slightly larger than that in the case of $CsCaI_3$ and given by Γ_{10K} = 710 cm^{-1}. However, the slight asymmetry cannot be explained by a mismatch between the ionic radii of Eu^{2+} and Sr^{2+} in this case, as they are almost equal ($r(Eu^{2+})$ = 1.17 Å, $r(Sr^{2+})$ = 1.18 Å).[29] Moreover, it turns out that the emission is slightly redshifted to the 5d–4f emission of Eu^{2+} in $CsCaI_3$, which does not correspond to the expectation when considering the decrease of the ionic radii from Ca^{2+} to Sr^{2+} and in turn the weaker crystal field splitting.

As for the other iodides, the fine structure due to the different ^7F_J levels is also observed in $CsSrI_3$ in all excitation bands (see Table 4 for their positions). The agreement with the values reported for Eu^{3+} is also satisfactory.[33] The Stokes shift determined thereof reads $\Delta S(2+,CsSrI_3)$ = 1090 cm^{-1}.

However, similar to the case of $CsMgI_3$:0.1% Eu^{2+} (*cf.* Fig. 5), another isolated band can be observed at 29 320 cm^{-1} (341 nm). This indicates a similarity of the site symmetry for the Eu^{2+} ions in $CsSrI_3$ compared to $CsMgI_3$. The larger disposal of the $[SrI_6]^-$ octahedra with respect to $CsCaI_3$ (see Fig. 3 and 4) thus seems to induce a trigonal distortion resulting in the sub site symmetry D_{3d} to first order. The subsequent symmetry distortion to the real site symmetry C_{2h} is assumed to be very weak and thus will be neglected for our considerations. With the assumption of D_{3d} as the site symmetry for the Eu^{2+} ions in $CsSrI_3$, the appearance of another isolated band in the excitation spectrum (see Fig. 7) seems plausible, leading to the splitting of the anticipated "t_{2g}" state into an a_{1g} and an e_g state. The excited e_g state retains its degeneracy. We will justify the order of the states a_{1g} and e_g shown in Fig. 7 in Section 4.2. From this interpretation, it is possible to deduce the trigonal crystal field splitting in $CsSrI_3$ given by $\varepsilon_{trig}(7,2+,CsSrI_3)$ = 3960 cm^{-1}.

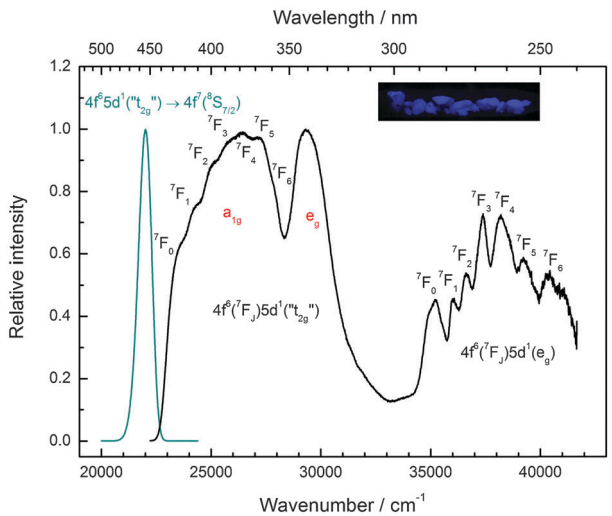

Fig. 7 Emission spectrum (cyan line, E_{ex} = 25 000 cm^{-1}) and excitation spectrum (black line, E_{em} = 21 980 cm^{-1}) of $CsSrI_3$:0.1% Eu^{2+} at 10 K. Note the splitting of the anticipated "t_{2g}" state into the trigonal field states a_{1g} and e_g. Inset: $CsSrI_3$:0.1% Eu^{2+} showing blue luminescence upon UV irradiation at room temperature.

Table 4 Positions of the $4f^6(^7F_J)5d^1$ states in $CsSrI_3$:Eu^{2+} (0.1%) and energy differences ΔE_{J-0} of the $4f^6(^7F_J)5d^1$ (J = 1–6) states relative to the $4f^6(^7F_0)5d^1$ state

$4f^6(^7F_J)5d^1$("t_{2g}")			$4f^6(^7F_J)5d^1(e_g)$		
State ^7F_J	Position/ cm^{-1}	ΔE_{J-0}/cm^{-1}	State ^7F_J	Position/ cm^{-1}	ΔE_{J-0}/cm^{-1}
$^7F_0$	23 100	0	$^7F_0$	35 300	0
$^7F_1$	23 610	510	$^7F_1$	35 980	680
$^7F_2$	24 350	1250	$^7F_2$	36 610	1310
$^7F_3$	25 070	1970	$^7F_3$	37 410	2110
$^7F_4$	26 190	3090	$^7F_4$	38 180	2880
$^7F_5$	27 300	4200	$^7F_5$	39 260	3960
$^7F_6$	27 930	4830	$^7F_6$	40 440	5140

3.6. Temperature-dependent emission

The temperature dependence of the 5d–4f emission of Eu^{2+} in the series $CsMI_3$ (M = Mg, Ca, Sr) was also investigated. The respective emission spectra are depicted in Fig. 8–10. In all three compounds, Eu^{2+} shows an intense luminescence even at room temperature and a slight blueshift with increasing temperature is observed. In the case of $CsMgI_3$:0.1% Eu^{2+} (see Fig. 8), an asymmetric wing of the emission on the red side of the spectrum evolves with increasing temperature. All these observations agree with the behavior we have already reported for the respective bromides.[17]

In Fig. 11, the evolution of the integrated intensities with increasing temperature is depicted. For all three compounds the photoluminescence signal is slightly quenched with higher temperatures. In fact, the integrated intensities of the emission of Eu^{2+} in $CsCaI_3$ and $CsSrI_3$ decrease to only 88% and 85% of the initial value when heated to 300 K, whereas in the case of $CsMgI_3$:0.1% Eu^{2+}, it decreases to 71%. This indicates that the quenching temperature $T_{1/2}$, at which the integrated intensity

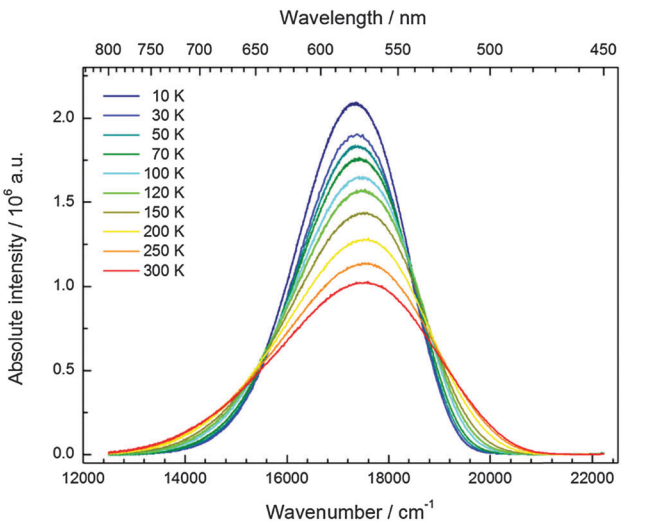

Fig. 8 Temperature-dependent emission spectra (E_{ex} = 24 390 cm^{-1}) of $CsMgI_3$:0.1% Eu^{2+}.

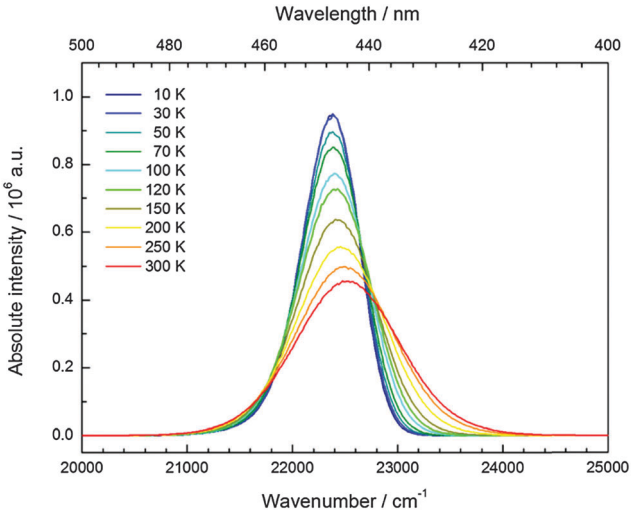

Fig. 9 Temperature-dependent emission spectra (E_{ex} = 25 640 cm^{-1}) of $CsCaI_3$:0.1% Eu^{2+}.

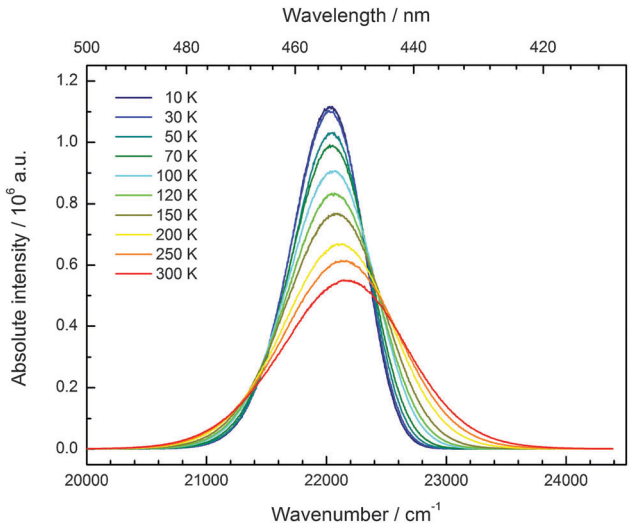

Fig. 10 Temperature-dependent emission spectra (E_{ex} = 25 000 cm^{-1}) of $CsSrI_3$:0.1% Eu^{2+}.

has reached 50% of the maximum signal, is well above 300 K in all three doped compounds. Unfortunately, we could not perform comparable measurements above 300 K so we are only able to state this about the quenching temperature. In fact, the low Stokes shifts for Eu^{2+} in these compounds and very low phonon energies in iodides (below 200 cm^{-1})[34] make non-radiative transitions very inefficient and a weak electron–phonon coupling should be expected. This behavior is clearly observed in Fig. 11.

3.7. Decay times

The decay curves of the luminescence signal of Eu^{2+} in $CsMI_3$ (M = Mg, Ca, Sr) are depicted in Fig. 12. They were recorded upon excitation into the "t_{2g}" states (λ_{ex} = 355 nm) at room temperature. All decay curves show a mono-exponential behavior in the recorded time range. Since the luminescence is also

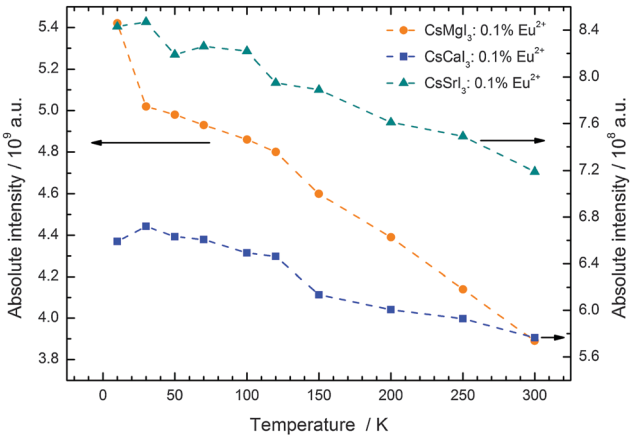

Fig. 11 Evolution of the integrated intensities of the 5d–4f emission of Eu^{2+} ions doped in the iodides $CsMI_3$ (M = Mg, Ca, and Sr).

not highly quenched at room temperature (see Section 3.3), it may also be assumed that the shortening of the decay time of Eu^{2+} by phonons is relatively small and, thus, a good estimate of the radiative lifetime is obtained by the room temperature measurements. Their values are compiled in Table 5.

From the decay times, it is possible to obtain direct information about the electric dipole matrix element $\mu_{5d\rightarrow 4f}$, since

$$\mu_{5d\rightarrow 4f} = -e\cdot|\langle 5d|r|4f\rangle| \quad (1)$$

where e is the elementary charge. The matrix element $\langle 5d|r|4f\rangle$ represents the radial integral between these two states and is related to the decay time by[35]

$$A_{tot}(7,2+,A) = \frac{1}{\tau} = 5.06\times 10^{-8}\cdot|\langle 5d|r|4f\rangle|^2\cdot\chi\cdot E_{em}{}^3(7,2+,A) \quad (2)$$

where A denotes the total transition probability per unit time, E_{em}(7,2+,A) is the emission energy of Eu^{2+} in compound A in

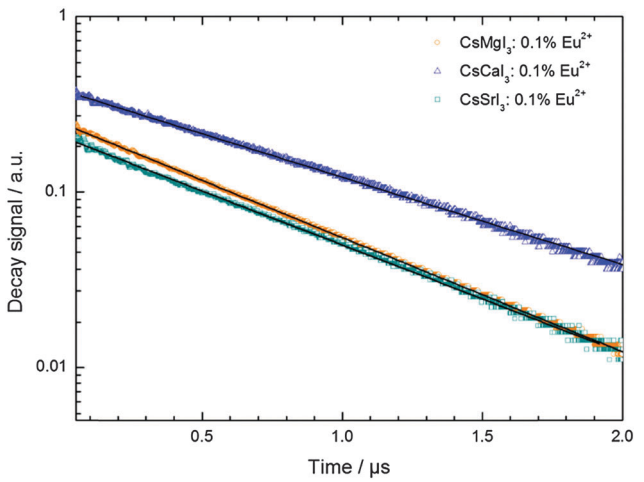

Fig. 12 Semi-log plot of the decay curves of $CsMI_3$:0.1% Eu^{2+} obtained upon excitation into the "t_{2g}" state (λ_{ex} = 355 nm) at room temperature. The solid black lines indicate exponential fits to the respective data.

Table 5 Decay times and radial integrals $|\langle 5d|r|4f\rangle|$ of $CsMI_3$:0.1% Eu^{2+} (M = Mg, Ca, and Sr) determined at room temperature

Compound	Decay time/ns	Radial integral $\|\langle 5d\|r\|4f\rangle\|$/Å
$CsMgI_3$:Eu^{2+}	667	1.03
$CsCaI_3$:Eu^2	875	0.50
$CsSrI_3$:Eu^2	707	0.70

cm^{-1} and χ is a correction factor that includes the refraction index n of the host medium,

$$\chi \approx \frac{n(n^2+2)^2}{9} \quad (3)$$

For $CsCaI_3$, a refraction index of 2.0 has been deduced from band structure calculations,[19] whereas for $CsSrI_3$, a refraction index of 1.79 was calculated.[36] Due to the similarity in the structures of $CsSrI_3$ and $CsMgI_3$, a refraction index of 1.79 was also assumed for $CsMgI_3$. With these values, it is possible to estimate the radial integrals for the 5d–4f transition for Eu^{2+} in the iodides $CsMI_3$ (M = Mg, Ca, Sr), as summarized in Table 5.

4. Discussion

4.1. Photoluminescence of Eu^{2+} doped in $CsMI_3$ (M = Mg, Ca, Sr)

Eu^{2+} shows very intense luminescence in the series $CsMI_3$ (M = Mg, Ca, Sr), which goes from blue in $CsCaI_3$ and $CsSrI_3$ to yellow in $CsMgI_3$. The important luminescence data obtained from the spectra presented in Section 3 are compiled in Table 6. As previously mentioned, all important equations to derive the respective values have already been described by us in another publication and can be found in the literature.[17] However, similar to the case of the respective bromides,[17] a fine structure due to the ^7F_J states (J = 0,...,6) arising from the $4f^6$ core in the excited $4f^65d^1$ state can be observed in the crystal field states "t_{2g}" and e_g. This clearly indicates that the exchange interaction between the 5d electron and the other six 4f electrons is very small.[32] Other conditions of such observations are high site symmetries, good crystal quality, low dopant concentrations and low temperature measurements.[27] Examples, in which Eu^{2+} is also known to exhibit well-resolved excitation spectra with such a fine structure, include $Sr_3(PO_4)_2$,[37] $Ba_2B_5O_9Br$[38] and binary alkali halides.[31] As the fine structure seems to be very well resolved even in the e_g state, which was so far only known for the alkali bromides and iodides,[31] we also presume that covalence of the bond between Eu^{2+} and the respective (halide) anions has an important effect upon the strength of the exchange interaction. This makes sense since a higher covalence exhibits a larger nephelauxetic effect and thus leads to a larger energy gap between the excited 4f states and 5d states inhibiting an admixture. Therefore, the exchange interaction will be small as well as the radiative lifetimes will be lowered. Both effects are indeed observed for the system $CsMI_3$ (M = Mg, Ca, Sr).

Since the covalence of the Eu–I bonds in these compounds should not vary very much, it may be assumed that the bond length and, thus, the size of the alkaline earth site are the most important factors in this case which influence the luminescence properties. As we will show below, this approximation is, however, too crude for $CsMgI_3$ and $CsSrI_3$.

We also attempted to analyze the emission energies $E_{em}(7,2+,A)$ and the positions of the $^7F_0$ levels within the "t_{2g}" and e_g states, denoted as $E_{ex}^{t_{2g}}(7,2+,{}^7F_0,A)$ and $E_{ex}^{e_g}(7,2+,{}^7F_0,A)$, respectively, with respect to the difference in the ionic radii between Eu^{2+} and the respective alkaline earth ion M^{2+} (M = Mg, Ca, Sr). The plots are illustrated in Fig. 13.

The curves shown in Fig. 13 nicely illustrate the nature of the different states and indicate the impact of the crystal structure upon the photoluminescence properties of Eu^{2+} in iodidoperovskites. Since the behavior of the emission energies and the excitation energies of the "t_{2g}" states is strikingly similar, it can be directly concluded that emission occurs from the lowest excited hypothetical "t_{2g}" state. It turns out for Eu^{2+}-activated $CsMgI_3$ and $CsSrI_3$ that both the energy of the "t_{2g}" states and the emission energy are lower than those in the case of $CsCaI_3$. The energies of the e_g state, however, remain relatively constant with respect to changes in the size of the alkaline earth site. This observation does not agree with the naive expectation that it should increase with decreasing Eu–I bond length due to the anti-bonding nature of the e_g state as it was observed in the respective bromidoperovskites.[17] This behavior can, however, be understood taking into account the large bond length between Eu^{2+} and I^-, which would be 3.37 Å according to the sum of the Shannon radii at 6-fold coordination.[29] With the

Table 6 Characteristic energies for Eu^{2+} extracted from the luminescence spectra of $CsMI_3$:0.1% Eu^{2+}. All values are in cm^{-1} and were recorded at 10 K. The addition (7,2+,A) was omitted here

$CsMI_3$	$E_{ex}^{t_{2g}}$	$E_{ex}^{e_g}$	E_{em}	D	ΔS	Γ_{10K}
$CsMgI_3$	21 200	35 240	17 330	12 800	3870	2430
$CsCaI_3$	23 680	34 970	22 370	10 320	1310	640
$CsSrI_3$	23 100	35 300	22 010	10 900	1090	710

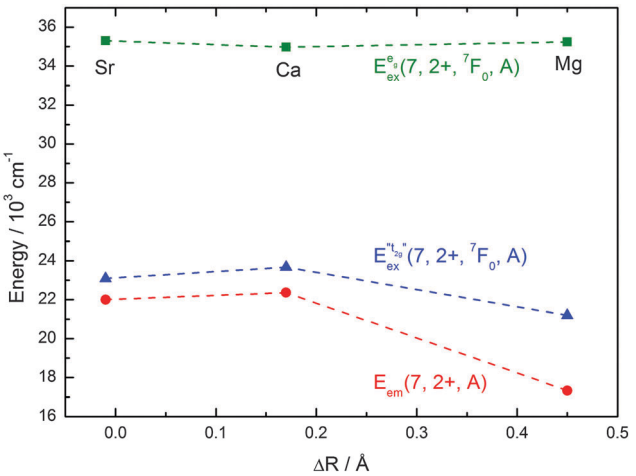

Fig. 13 Variation of the emission energies $E_{em}(7,2+,A)$ and the energies of the $^7F_0$ level within the hypothetical "t_{2g}" and e_g states, $E_{ex}^{t_{2g}}(7,2+,{}^7F_0,A)$ and $E_{ex}^{e_g}(7,2+,{}^7F_0,A)$, with the difference in Shannon radii ΔR between Eu^{2+} and the alkaline earth ion in $CsMI_3$ (M = Mg, Ca, and Sr).[29]

anti-bonding nature of the e_g this value should yet be larger. Therefore, the repulsive interaction between the 5d electron of Eu^{2+} and the 5p electrons of I^- ions is negligibly small giving rise to the relatively constant behavior.

A more detailed view in Fig. 13 already reveals the special role that $CsCaI_3$ plays within this series. In fact, the emission energy and the energy of the $^7F_0$ levels within the t_{2g} state go through a maximum, whereas the respective energy of the $^7F_0$ levels within the e_g state goes through a minimum in that case. We emphasize again to keep in mind that in the case of $CsCaI_3$, it is valid to speak of a t_{2g} state. The special dependence of the energies upon the size of the alkaline earth site can be directly correlated with the structures of the iodides. As indicated in Section 3.1, the tendency of tilting of the $[EuI_6]^{4-}$ octahedra increases from $CsCaI_3$ over $CsSrI_3$ to $CsMgI_3$. In the last compound, the octahedra are face-sharing (see Fig. 2). This goes along with an increasing trigonal distortion of the $[EuI_6]^{4-}$ octahedra to D_{3d} symmetry and the fact that the Eu^{2+} ions experience stronger repulsive forces due to the alkaline earth ions in the second coordination sphere. This is not the case for $CsCaI_3$. The subsequent symmetry reduction to the real site symmetry C_{2h} in $CsSrI_3$ is assumed to be very weak and will be neglected for the following considerations. The t_{2g} state splits into an a_{1g} and an e_g state in D_{3d} symmetry. Therefore, the lowest excited state and the emission energies of Eu^{2+} in $CsMgI_3$ and $CsSrI_3$ should be lower than those in the case of $CsCaI_3$. These aspects are well reproduced by the spectra (see Fig. 13) and are, in fact, the reason for the strange behavior of $CsSrI_3$:Eu^{2+} showing a slightly redshifted emission with respect to $CsCaI_3$:Eu^{2+}. In the latter Eu^{2+}-activated compound, the effect of trigonal distortion is negligibly small, as we will also show in the following section.

The discussion above indicates that the size of the alkaline earth site is not the only important parameter of the luminescence properties of Eu^{2+} in iodidoperovskites. Especially in the case of $CsMgI_3$:Eu^{2+}, the emission is extraordinarily redshifted. We have reported a similar behavior for $CsMgBr_3$:Eu^{2+}.[17] Both compounds exhibit a high anisotropy and a pseudo-one-dimensional characteristic along the hexagonal *c* axis. Together with the small size of the Mg^{2+} site inducing a large crystal field splitting, the anisotropy synergetically leads to a large redshift. It has been discussed in the literature that the structural feature of linear chains induces a preferential orientation of one of the 5d orbitals into the direction of the chain.[37,39] Due to the similar behavior of $CsSrI_3$:Eu^{2+} with respect to $CsMgI_3$:Eu^{2+} and the observed splitting in the excitation spectra, we assign the extraordinary redshift for $CsMgI_3$:Eu^{2+} to the effect of the trigonal distortion induced by the tilts of the $[EuI_6]^{4-}$ octahedra rather than to a preferential orientation of the 5d orbitals. In general, this is an important issue for applications especially in the LED technology, where it is desired to have green- to red-emitting phosphors excitable in the blue range. Therefore, not only the size of the alkaline earth site can help here but also a larger anisotropy and with that, a larger distortion.

Based on this interpretation, it is possible to deduce the position of the undistorted "t_{2g}" state and, thus, the octahedral crystal field splitting, $\varepsilon_{cfs}^{undist.}(7,2+,A)$ = 10 Dq, without distortion. Since the energy of the barycenter of the undistorted "t_{2g}" state is conserved, the resulting a_{1g} state is lowered by 2/3 $\varepsilon_{trig}(7,2+,A)$, whereas the resulting e_g state is increased by 1/3 $\varepsilon_{trig}(7,2+,A)$. Assuming that the distortion of the initial e_g state in O_h symmetry is negligible, the octahedral crystal field splitting for the undistorted case can be derived as follows:

$$\varepsilon_{cfs}^{undist.}(7,2+,A) = E_{ex}^{e_g}(7,2+,A) - \left(E_{a_{1g}}^{trig}(7,2+,A) + \frac{2}{3}\varepsilon_{trig}(7,2+,A)\right) \quad (4)$$

$$\varepsilon_{cfs}^{undist.}(7,2+,A) = E_{ex}^{e_g}(7,2+,A) - \left(E_{e_g}^{trig}(7,2+,A) - \frac{1}{3}\varepsilon_{trig}(7,2+,A)\right) \quad (5)$$

where $E_{ex}^{e_g}(7,2+,A)$ is the average energy of the excitation band assigned to the e_g state in O_h symmetry and $E_{a_{1g}}^{trig}(7,2+,A)$ and $E_{e_g}^{trig}(7,2+,A)$ are the average energies of the respective trigonal states as found in the excitation spectra of the compounds. The values for the octahedral crystal field splitting without distortion are compiled in Table 7.

As expected, the values in Table 7 increase with decreasing size of the alkaline earth site, thus inducing a smaller Eu–I bond length. Upon comparison with the 10 *Dq* values known from the respective bromidoperovskites,[17] the derived values for the iodides are all smaller. This is in agreement with theoretical considerations since I^- is a larger ion and more polarizable and, thus, a softer ligand. It should be noted, however, that for $CsMgBr_3$:Eu^{2+}, the crystal field splitting was directly derived without considering trigonal distortion.[17] Therefore, the corrected value for 10 Dq in the case of $CsMgBr_3$:Eu^{2+} will be smaller (13 230 cm^{-1}). It is, however still larger than the value of the respective iodide. The crystal field splitting derived using eqn (4) and (5) is in the range known from alkali halides[31] making our interpretation plausible.

4.2. Energetic order of trigonal crystal field states in $CsMgI_3$:Eu^{2+} and $CsSrI_3$:Eu^{2+}

Throughout this paper, we argued that the trigonal distortion leads to a splitting of the t_{2g} state into an a_{1g} and an e_g state with the latter being higher in energy. In this section, we want to justify this statement using the angular overlap model (AOM) known from ligand field theory. A well-written review about this approach has been published by Schäffer[40] and the reader can refer to it for the details of this approach. Since the 5d orbitals are much more diffuse and more involved in metal–ligand bonding than the 4f orbitals of Eu^{2+}, the latter were neglected

Table 7 Deduced values of the undistorted octahedral crystal field splitting, $\varepsilon_{cfs}^{undist.}(7,2+,A)$ = 10 Dq for $CsMI_3$:0.1% Eu^{2+} (M = Mg, Ca, and Sr)

Compound	$\varepsilon_{cfs}^{undist.}(7,2+,A)/cm^{-1}$
$CsMgI_3$:Eu^{2+}	11 300
$CsCaI_3$:Eu^{2+} [a]	11 050[a]
$CsSrI_3$:Eu^{2+}	9600

[a] No trigonal distortion in this case.

in the AOM approximation. In the case of $CsMgI_3:Eu^{2+}$ and $CsSrI_3:Eu^{2+}$, the trigonal distortion of the $[EuI_6]^{4-}$ octahedra evolves along the C_3 axis, thus leading to the disposal of the ligands with respect to the normal z axis by a small polar angle Θ (see Fig. 14). The strong tilting pattern of the respective octahedra in the structures of $CsMgI_3$ and $CsSrI_3$ (see Fig. 2 and 4) induces a stronger repulsion between the ligands, which makes the trigonal distortion also plausible from an electrostatic perspective.

For the AOM approximation, it is assumed that the Eu–I bond lengths do not change during the trigonal distortion, *i.e.* only the angular part of the overlap integral is important in this consideration. If the Eu^{2+} ion is placed into the origin of the coordinate system, the positions of the ligands can be parametrized by the disposal Θ of the Eu–I bond with respect to the z axis and their azimuthal angle Φ relative to the x axis. The numbering of the ligands as denoted in Fig. 14 leads to the parametrization shown in Table 8.

The distortion angle Θ is not known quantitatively, thus, it will be denoted by a small angle θ. With the parametrization in Table 8 the factors by which the angular overlap integrals are diminished from the maximum value can be deduced in the coordination frame shown in Fig. 14. They arise due to the fact that for every spherically symmetric ligand, the coordination frame has to be rotated such that the 5d orbitals have maximum overlap with the ligand orbitals. This procedure leads to a 5×5 transformation matrix that has to be evaluated for every ligand separately. Its general form has been deduced by Schäffer.[41]

For the calculation in the case of $CsMgI_3$ and $CsSrI_3$, some other assumptions have still to be taken into account. Within the AOM approximation, only σ- and π-like interactions are considered and parametrized by the interaction terms e_σ and e_π. Moreover, for small angles θ, the functions $\sin\theta$ and $\cos\theta$ can be approximated very well by their Taylor expansions up to second order. With these assumptions, the energies of the $5d_{xz}$, $5d_{xy}$ and $5d_{yz}$ orbitals transforming as t_{2g} states in a perfect octahedral environment can be evaluated during the trigonal distortion:

$$\varepsilon_{xz} = 4e_\pi + \theta^2(9e_\sigma - 11e_\pi) \quad (6)$$

$$\varepsilon_{yz} = 4e_\pi + \theta^2(9e_\sigma - 11e_\pi) \quad (7)$$

$$\varepsilon_{xy} = 4e_\pi - 2e_\pi\theta^2 \quad (8)$$

In accordance with the group theoretical expectation, $5d_{xz}$ and $5d_{yz}$ degenerate forming the e_g state, whereas the $5d_{xy}$ orbital transforms as an a_{1g} state in D_{3d} symmetry and affords a different energy in the AOM. It should be noted that no assumptions about the symmetry and degeneracy of states have been included into this calculation, *i.e.* the results of the AOM are totally independent of the group theoretical considerations. The energy splitting between the a_{1g} and the e_g state is given by

$$\varepsilon_{trig}^{AOM}(7,2+) = 9\theta^2(e_\sigma - e_\pi) \quad (9)$$

Since I^- ions are weak π donors, it may be assumed that $e_\sigma \gg e_\pi$. Thus, eqn (9) affords a positive result indicating that the a_{1g} state is lower in energy than the e_g state. However, eqn (9) allows another conclusion as well. As the degree of tilt of the $[MI_6]^{4-}$ octahedra (M = Mg, Ca, and Sr) increases in the series $CsCaI_3 < CsSrI_3 < CsMgI_3$, the repulsion between the I^- ligands also increases, and so does θ. In the case of $CsCaI_3:Eu^{2+}$, θ is negligibly small and therefore, no splitting due to trigonal distortion is observed in the excitation spectra (see Fig. 9). The $5d_{xz}$, $5d_{xy}$ and $5d_{yz}$ orbitals degenerate in that case forming the t_{2g} manifold with an energy of $4e_\pi$. This agrees with the well-known result from ligand field theory.[40] In the cases of $CsMgI_3:Eu^{2+}$ and $CsSrI_3:Eu^{2+}$, however, the angle θ has to be taken into account. The $[MgI_6]^{4-}$ octahedra in $CsMgI_3$ are tilted to a much larger degree than the respective octahedra in $CsSrI_3$. Therefore, the splitting due to the trigonal distortion should be lower in the latter compound, which is indeed observed (see Table 9).

The behavior of the curves shown in Fig. 13 is also well understood in terms of the AOM. When regarding eqn (6)–(8), it turns out that the energies of the hypothetical "t_{2g}" state, $E_{ex}^{t_{2g}}(7,2+,{}^7F_0,A)$, should decrease with increasing θ. This is exactly the observed behavior. $CsCaI_3:Eu^{2+}$ provides the limiting case $\theta \to 0$, thus leading to a maximum for $E_{ex}^{t_{2g}}(7,2+,{}^7F_0,A)$ in this series.

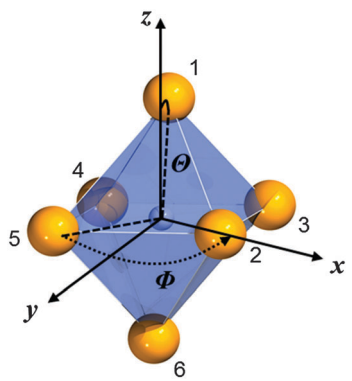

Fig. 14 Numbering of the ligands and their respective angular positions within the equatorial plane (Φ) and relative to the normal z axis (Θ) of the $[EuI_6]^{4-}$ octahedron in $CsMgI_3$ and $CsSrI_3$.

Table 8 Parametrization of the polar angle Θ and the azimuthal angle Φ of the ligands as denoted in Fig. 13

	L_1	L_2	L_3	L_4	L_5	L_6
Φ	$\pi/4$	0	$\pi/2$	π	$3\pi/2$	$5\pi/4$
Θ	θ	$\pi/2 - \theta$	$\pi/2 + \theta$	$\pi/2 + \theta$	$\pi/2 - \theta$	$\pi + \theta$

Table 9 Experimental values for the trigonal crystal field splitting of the "t_{2g}" manifold, as deduced from the excitation spectra in $CsMI_3:Eu^{2+}$ (M = Mg, Ca, and Sr)

Compound	$\varepsilon_{trig}(7,2+,A)/cm^{-1}$
$CsMgI_3:Eu^{2+}$	4310
$CsCaI_3:Eu^{2+}$	—
$CsSrI_3:Eu^{2+}$	3960

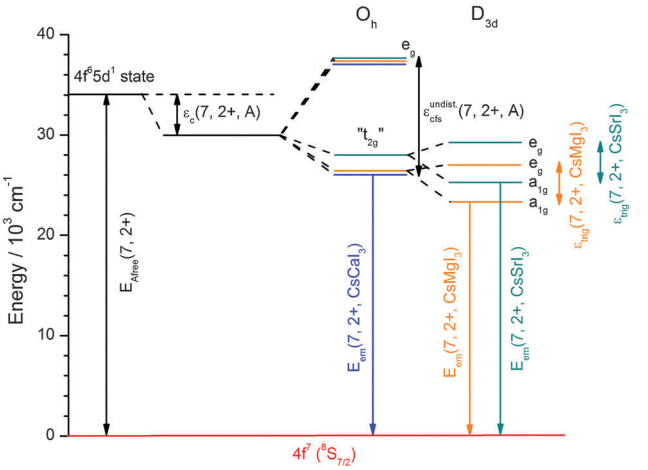

Fig. 15 Schematic energy level scheme for the 5d states of Eu^{2+} and the resulting luminescence in $CsMI_3$:Eu^{2+} (M = Mg, Ca, and Sr). The centroid shift as drawn was determined from the average position of the "t_{2g}" state and should only be considered qualitatively.

Fig. 15 finally represents a summarizing schematic overview of the evolution of the 5d states of Eu^{2+} in $CsMI_3$ (M = Mg, Ca, and Sr). It shows the irregular behavior of the emission energies illustratively. The centroid shift, $\varepsilon_c(7,2+,A)$, should only be regarded qualitatively and was intentionally not determined for iodidoperovskites. Since a strong degree of tilt for the $[MI_6]^{4-}$ octahedra is not reasonable in terms of Pauling's rules[42] due to the larger repulsion, this effect indicates a larger covalence of the M–I bond and thus, the Eu–I bond. Moreover, the effect of trigonal distortion has to be included into the formula such that a simple approach as attempted for the bromidoperovskites[17] does not seem very reasonable. We will discuss the effect of higher covalence of the Eu–I bond in $CsMgI_3$:Eu^{2+} and $CsSrI_3$:Eu^{2+} in terms of the decay times in Section 4.4.

4.3. Temperature-dependent emission

All Eu^{2+}-activated iodidoperovskites $CsMI_3$ (M = Mg, Ca, and Sr) show efficient luminescence even at room temperature. As we have already indicated in Section 3.3, the quenching temperature $T_{1/2}$, at which the integrated intensity has decreased to 50% of its initial value at 10 K, is well above 300 K. In fact, the intensities in $CsCaI_3$:Eu^{2+} and $CsSrI_3$:Eu^{2+} at room temperature only decrease to 88% and 85%, respectively, compared to their 10 K values. Together with the low Stokes shifts, this indicates a weak electron–phonon coupling. This is predominantly due to the fact that the highest phonon energy in iodides is relatively low (below 200 cm^{-1}).[34] The 5d–4f emission of Eu^{2+} in $CsCaI_3$ and $CsSrI_3$ exhibits a blueshift with higher temperatures, which arises due to the thermal population of the higher ^7F_J levels within the lowest excited 5d state.

Interestingly, the Stokes shift $\Delta S(2+,CsMgI_3)$ and the FWHM Γ at 10 K are both very large in the case of $CsMgI_3$:Eu^{2+} (see Table 6). Moreover, the emission is highly asymmetric. This behavior is already familiar from $CsMgBr_3$:Eu^{2+}.[17] As a possible explanation anomalous luminescence could be assumed, which arises if the 5d states are closely located at the bottom or inside of the conduction band of the host lattice. Anomalous luminescence of Eu^{2+} is typically characterized by Stokes shifts in the range of 4000–10 000 cm^{-1}, large FWHMs (4000–6000 cm^{-1}), shortened decay times and low quenching temperatures $T_{1/2}$.[43] However, the large covalence of the Eu–I bond in $CsMgI_3$ will shift the 5d states to low energies. Due to that fact and the large crystal field splitting due to the small Mg^{2+} site and the trigonal distortion, it does not seem very probable that anomalous luminescence occurs in this compound. The experimental results also contradict the presence of anomalous luminescence since the luminescence is still very efficient even at room temperature and a fine structure due to the ^7F_J levels can even be observed in the high-energy excitation band assigned to the e_g crystal field state (see Fig. 5 and 11). Thus, we exclude anomalous luminescence of Eu^{2+} in $CsMgI_3$. Nevertheless, the large Stokes shift and FWHM at 10 K indicate a large reorganization of the electron density in the excited state. Obviously, this is related to the huge difference between the ionic radii of Mg^{2+} and Eu^{2+} (ΔR = 0.45 Å[29]) and the relatively short Mg–I bond length (see Table 1). Upon excitation into the diffuse 5d orbitals of Eu^{2+}, the Eu–I bond length is expected to change drastically inducing the large Stokes shift and, subsequently, the large FWHM. A quantitative correlation between the Stokes shift and the size of the alkaline earth site is, however, not very reasonable since it is not known whether the Eu–I distance increases or decreases in the excited state. In general, an increase of the bond length is assumed due to the more antibonding nature of the excited state. However, as it has been shown for the Ce^{3+}-activated elpasolite $CsNaLuCl_6$ by pressure-dependent luminescence measurements, the potential surface of the excited 5d state can also be located at lower metal–ligand distances than for the ground state.[44]

For $CsSrI_3$:Eu^{2+}, however, the Stokes shift $\Delta S(2+,CsSrI_3)$ and the FWHM Γ at 10 K are very low (see Table 6), although the structure of the host compound is very similar to that of $CsMgI_3$. Moreover, a lower Stokes shift of 1090 cm^{-1} and 1420 cm^{-1},[17] respectively, is observed compared to $CsSrBr_3$:Eu^{2+}. In general, an increase of the Stokes shift is expected upon increase of the polarizability of the ligands. This trend is clearly observed when comparing $CsCaBr_3$:Eu^{2+} ($\Delta S(2+,CsCaBr_3)$ = 1080 cm^{-1} (ref. 17)) with $CsCaI_3$:Eu^{2+} ($\Delta S(2+,CsCaI_3)$ = 1310 cm^{-1}, see Table 6). Our explanation for the reverse effect in the Sr-based compounds relies on the fact that the average Sr–I bond length is relatively large (3.37 Å, see Table 1[24]). Since Eu^{2+} ions have approximately the same ionic radius as Sr^{2+} ions, they will be readily incorporated into the structure without severe distortion effects. If the Eu–I bond length is therefore relatively large in the ground state, an excitation into the 5d states will not change the bond length drastically and vibrational relaxation upon reorganization of the electron density is highly reduced giving rise to a small Stokes shift. Calculations of the electron density distribution in the ground and the first excited state and the resulting bond lengths could give some further insight here.

4.4. Decay times and radial integrals

The measured decay times and deduced values of the radial integrals (see Table 5) of Eu^{2+} in $CsMI_3$ (M = Mg, Ca, Sr) are in

good agreement with the values reported in the literature.[35] Although they have been measured at room temperature, the low vibrational energy in iodides makes vibrational coupling rather inefficient such that the decay time is not significantly shortened with respect to temperatures as low as 10 K. Their dependence upon the size of the alkaline earth site is plotted in Fig. 16.

The behavior of the decay times of Eu^{2+} with varying differences in ionic radii of Eu^{2+} and the alkaline earth ion is very similar to the variation of the emission energies and thus, the energies $E_{ex}^{t_{2g}}(7, 2+, {}^7F_0, A)$ indicate that the "t_{2g}" state is the emissive state. As has already been discussed above, Eu^{2+}-activated $CsSrI_3$ and $CsMgI_3$ show an exceptional behavior also in the decay times and conclusively, also in the radial integrals. In fact, the decay times of Eu^{2+} in these two compounds are very short compared to the values known from oxides.[35] Obviously, this is related to the larger disposal of the octahedra in both structures. Such disposal is related to a larger covalence of the Eu–I bond. Due to the nephelauxetic effect, this lowers the barycenter of the 5d states inhibiting an admixture with the excited $4f^7$ states of Eu^{2+}. Thus, the decay times of $CsMI_3$:Eu^{2+} (M = Mg, Sr) are lowered compared to the decay time of Eu^{2+} in $CsCaI_3$.

The decay times detected for $CsCaI_3$:Eu^{2+} and $CsSrI_3$:Eu^{2+} are shorter compared to the respective bromides,[17] in accordance with the expectations regarding the higher covalence and the stronger nephelauxetic effect in iodides. In the case of $CsMgI_3$:Eu^{2+}, the decay time is strikingly similar to the value found for $CsMgBr_3$:Eu^{2+}.[17] Taking the fact into account that the "t_{2g}" excitation band is at almost the same energy in both compounds, one may conclude that the synergic effect of covalence and trigonal distortion leads to roughly the same position of the lowest excited state of Eu^{2+} in $CsMgBr_3$ and $CsMgI_3$ and thus, to a similar decay time.

The radial integrals are also in a reasonable range. They are significantly larger for $CsMgI_3$:Eu^{2+} and $CsSrI_3$:Eu^{2+} than for $CsCaI_3$:Eu^{2+}. This indicates a larger overlap between the 4f and the 5d wavefunctions in the former two compounds, which is induced by the increasing anisotropy in both structures. In the case of $CsMgI_3$:Eu^{2+}, the small size of the Mg^{2+} site still increases the value of the radial integral and thus, lowers the decay time.

In the cases of $CsCaI_3$:Eu^{2+} and $CsSrI_3$:Eu^{2+}, the low Stokes shifts allow the possibility of self-absorption that might lead to lengthening of the decay time. This effect can be excluded here, however, due to the low concentration of only 0.1 mol% that leads to a high probability of isolation of the Eu^{2+} ions.

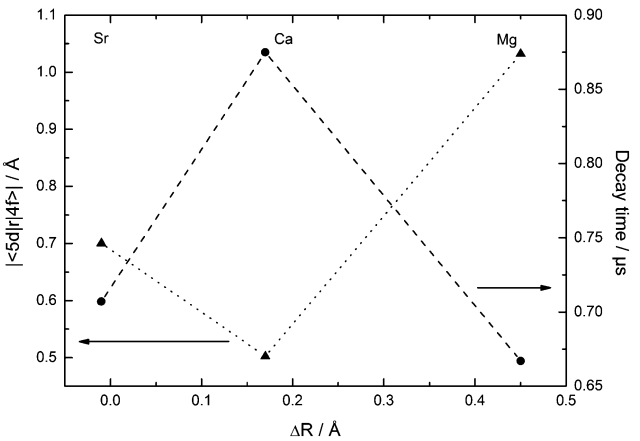

Fig. 16 Dependence of the decay times τ (●, dashed curve) and radial integrals $|\langle 5d|r|4f\rangle|$ (▲, dotted curve) of Eu^{2+} upon the size of the alkaline earth site in $CsMI_3$ (M = Mg, Ca, and Sr).

5. Conclusions

The photoluminescence properties of Eu^{2+}-activated $CsMI_3$ (M = Mg, Ca, Sr) were presented and analyzed in detail. The crystal structures of the compounds can be derived from a perovskite structure type with six-fold coordinated alkaline earth sites substituted by Eu^{2+}. All emission spectra are characterized by an asymmetric Gaussian-shaped band that can be assigned to $4f^6({}^7F_J)5d^1 \rightarrow 4f^7({}^8S_{7/2})$ transitions. All excitation spectra provide a distinct fine structure in both the "t_{2g}" and the e_g state during approximation of an octahedral symmetry for the Eu^{2+} ions. It can be assigned to the different ^7F_J levels arising from $4f^6$ core in the excited state using a decoupled scheme and thus assuming a weak exchange interaction between the 4f electrons and the 5d electron. This behavior is in agreement with the behavior observed for the respective bromides[17] and is otherwise only known for the alkali bromides and iodides.[31] In the cases of Eu^{2+}-activated $CsMgI_3$ and $CsSrI_3$, the excitation spectra reveal a non-negligible trigonal distortion of the $[EuI_6]^{4-}$ octahedra leading to a splitting of the supposed "t_{2g}" state into an a_{1g} and an e_g state. Their energetic order has been justified in terms of the angular overlap model of ligand field theory. The trigonal distortion leads to several irregular effects like a redshifted emission and excitation of Eu^{2+} in $CsSrI_3$ with respect to Eu^{2+}-activated $CsCaI_3$ that would not be anticipated assuming a simple octahedral symmetry. The asymmetry of the emission of Eu^{2+} in $CsMgI_3$ and $CsSrI_3$ can be understood taking the splitting of the "t_{2g}" state into account.

An analysis of the behavior of the emission and excitation energies of Eu^{2+} ions dependent upon the size of the alkaline earth site substituted indicates that emission occurs from the lowest excited supposed "t_{2g}" state. It turns out that the lowest excited states are slightly bonding whereas the high-energy e_g state is almost non-bonding due to the large Eu–I bond length in the excited state.

All Eu^{2+}-activated iodides presented in this paper show very efficient photoluminescence even at room temperature. The quenching temperatures $T_{1/2}$ are all well above room temperature, which is easily understood taking the low phonon energies in iodides into account that makes vibrational coupling rather inefficient. The Stokes shifts are also rather small except in the case of $CsMgI_3$:Eu^{2+}. Here, the large Stokes shift is most probably induced by the large amount of reorganization of the electron density in the excited state due to the low Eu–I bond length in the ground state.

The values of the decay times are all shorter, or, in the case of $CsMgI_3:Eu^{2+}$, similar to the decay times detected for the respective bromides.[17] This is in accordance with the expectations. The decay times of $CsMgI_3:Eu^{2+}$ and $CsSrI_3:Eu^{2+}$ are extraordinarily short, which can also be correlated with their special structure. In fact, the larger disposal of the octahedra in these compounds indicates a larger covalence of the M–I bond and thus, the Eu–I bond, which is directly reflected in the lower decay times relative to $CsCaI_3:Eu^{2+}$. In general, the materials investigated in this work allow an extremely detailed insight into the Eu^{2+} structure–luminescence relationship due to the high resolution of the spectra and may, thus, serve as a textbook example in this context.

Acknowledgements

We are grateful to Prof. Dr Richard Dronskowski and Prof. Dr Andrei Tchougréeff from RWTH Aachen for their enormous help with the angular overlap model considerations.

Notes and references

1 T. Kobayasi, S. Mroczkowski, J. F. Owen and L. H. Brixner, *J. Lumin.*, 1980, **21**, 247.
2 A. Ellens, A. Meijerink and G. Blasse, *J. Lumin.*, 1994, **59**, 293.
3 D. K. Sardar, W. A. Sibley and R. Alcala, *J. Lumin.*, 1982, **27**, 401.
4 C. Braun, M. Seibald, S. L. Börger, O. Oeckler, T. D. Boyko, A. Moewes, G. Miehe, A. Tücks and W. Schnick, *Chem. – Eur. J.*, 2010, **16**, 9646.
5 Y. Q. Li, J. E. J. v. Steen, J. W. H. v. Krevel, G. Botty, A. C. Delsing, F. J. DiSalvo, G. D. With and H. T. Hintzen, *J. Alloys Compd.*, 2006, **417**, 273.
6 V. Bachmann, C. Ronda, O. Oeckler, W. Schnick and A. Meijerink, *Chem. Mater.*, 2009, **21**, 316.
7 V. Bachmann, T. Jüstel, A. Meijerink, C. Ronda and P. J. Schmidt, *J. Lumin.*, 2006, **121**, 441.
8 N. Yamashita, O. Harada and K. Nakamura, *Jpn. J. Appl. Phys.*, 1995, **34**, 5539.
9 J. O. Rubio, *J. Phys. Chem. Solids*, 1991, **52**, 101.
10 P. Dorenbos, *J. Lumin.*, 2003, **104**, 239.
11 G. Blasse, *Phys. Status Solidi B*, 1973, **55**, K131.
12 C. Wickleder, *J. Alloys Compd.*, 2000, **300**, 193.
13 D. H. Gahane, N. S. Kokode, B. M. Bahirwar and S. V. Moharil, *Phys. Procedia*, 2012, **29**, 42.
14 A. Y. Grippa, N. V. Rebrova, T. E. Gorbacheva, V. Y. Pedash, N. N. Kosinov, V. L. Cherginets, V. A. Tarasov, O. A. Tarasenko and A. V. Lopin, *J. Cryst. Growth*, 2013, **371**, 112.
15 V. L. Cherginets, A. Y. Grippa, T. P. Rebrova, Y. N. Datsko, T. V. Ponomarenko, N. V. Rebrova, N. N. Kosinov and O. V. Zelenskaya, *Funct. Mater.*, 2012, **19**, 429.
16 V. L. Cherginets, N. V. Rebrova, A. Y. Grippa, Y. N. Datsko, T. V. Ponomarenko, V. Y. Pedash, N. N. Kosinov, V. A. Tarasov, O. V. Zelenskaya, I. M. Zenya and A. V. Lopin, *Mater. Chem. Phys.*, 2014, **143**, 1296.
17 M. Suta, P. Larsen, F. Lavoie-Cardinal and C. Wickleder, *J. Lumin.*, 2014, **149**, 35.
18 M. Zhuravleva, B. Blalock, K. Yang, M. Koschan and C. L. Melcher, *J. Cryst. Growth*, 2012, **352**, 115.
19 M. Tyagi, M. Zhuravleva and C. L. Melcher, *J. Appl. Phys.*, 2013, **113**, 203504.
20 K. Yang, M. Zhuravleva and C. L. Melcher, *Phys. Status Solidi RRL*, 2011, **5**, 43.
21 H. Wei, M. Zhuravleva, K. Yang and C. L. Melcher, *J. Cryst. Growth*, 2013, **384**, 27.
22 M. D. Taylor and C. P. Carter, *J. Inorg. Nucl. Chem.*, 1962, **24**, 387.
23 G. L. McPherson, A. M. McPherson and J. L. Atwood, *J. Phys. Chem. Solids*, 1980, **41**, 495.
24 G. Schilling and G. Meyer, *Z. Anorg. Allg. Chem.*, 1996, **622**, 759.
25 S. García-Revilla and R. Valiente, *J. Phys.: Condens. Matter*, 2006, **18**, 11139.
26 S. García-Revilla, F. Rodríguez and R. Valiente, *J. Lumin.*, 2008, **128**, 937.
27 P. Dorenbos, *J. Phys.: Condens. Matter*, 2003, **15**, 575.
28 P. Dorenbos, *J. Phys.: Condens. Matter*, 2003, **15**, 4797.
29 R. D. Shannon, *Acta Crystallogr., Sect. A: Cryst. Phys., Diffr., Theor. Gen. Crystallogr.*, 1976, **32**, 751.
30 H. J. Seo, W. S. Zhang, T. Tsuboi, S. H. Doh, W. G. Lee, H. D. Kang and K. W. Jang, *J. Alloys Compd.*, 2002, **344**, 268.
31 J. Hernandez, W. K. Cory and J. Rubio, *J. Chem. Phys.*, 1980, **72**, 198.
32 F. M. Ryan, W. Lehmann, D. W. Feldman and J. Murphy, *J. Electrochem. Soc.*, 1974, **121**, 1475.
33 W. T. Carnall, G. L. Goodman, K. Rajnak and R. S. Rana, *J. Chem. Phys.*, 1989, **90**, 3443.
34 K. Wakamura, *Phys. Rev. B: Condens. Matter Mater. Phys.*, 1997, **56**, 11593.
35 S. H. M. Poort, A. Meijerink and G. Blasse, *J. Phys. Chem. Solids*, 1997, **58**, 1451.
36 G. Shwetha and V. Kanchana, *Phys. Rev. B: Condens. Matter Mater. Phys.*, 2012, **86**, 115209.
37 S. H. M. Poort, J. W. H. v. Krevel, R. Stomphorst, A. P. Vink and G. Blasse, *J. Solid State Chem.*, 1996, **122**, 432.
38 A. Meijerink and G. Blasse, *J. Lumin.*, 1989, **43**, 283.
39 S. H. M. Poort, W. P. Blokpoel and G. Blasse, *Chem. Mater.*, 1995, **7**, 1547.
40 C. E. Schäffer, *Pure Appl. Chem.*, 1970, **24**, 361.
41 C. E. Schäffer, *Struct. Bonding*, 1968, **5**, 68.
42 L. Pauling, *J. Am. Chem. Soc.*, 1929, **51**, 1010.
43 P. Dorenbos, *J. Phys.: Condens. Matter*, 2003, **15**, 2645.
44 R. Valiente, F. Rodríguez, J. González, H. U. Güdel, R. Martín-Rodríguez, L. Nataf, M. N. Sanz-Ortiz and K. Krämer, *Chem. Phys. Lett.*, 2008, **481**, 149.